Dielectric and Thermal Effects on the Optical Properties of Natural Dyes: A Case Study on Solvated Cyanin

Osman Barış Malcıoğlu,[†] Arrigo Calzolari,*,[‡,#] Ralph Gebauer,[‡,§] Daniele Varsano,[‖] and Stefano Baroni[†,‡]

[†]SISSA − Scuola Internazionale Superiore di Studi Avanzati, I-34136 Trieste, Italy

[‡]CNR-IOM DEMOCRITOS Simulation Center, c/o SISSA, I-34136 Trieste, Italy

[§]ICTP − The Abdus Salam International Centre for Theoretical Physics, I-34151 Trieste, Italy

[‖]Dipartimento di Fisica, Università "La Sapienza", 00185 Roma, Italy and Centro S3, CNR-Nano Istituto di Nanoscienze, I-41100 Modena, Italy

S *Supporting Information*

ABSTRACT: The optical properties of the flavylium state of the cyanin dye are simulated numerically by combining Car−Parrinello molecular dynamics and linear-response time-dependent density functional theory calculations. The spectrum of the dye calculated in the gas phase is characterized by two peaks in the yellow and in the blue (green and violet), using a GGA-PBE (hybrid-B3LYP) DFT functional, which would bring about a greenish (bright orange) color incompatible with the dark purple hue observed in nature. Describing the effect of the water solvent through a polarizable continuum model does not modify qualitatively the resulting picture. An explicit simulation of both solvent and thermal effects using ab initio molecular dynamics results instead in a spectrum that is compatible with the observed coloration. This result is analyzed in terms of the spectroscopic effects of the molecular distortions induced by thermal fluctuations.
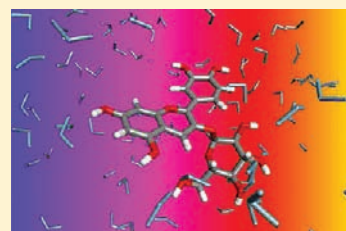
■ INTRODUCTION

Molecular dyes have received great attention in the last few years because of their application as pigments in many food, pharmaceutical, and textile preparations. However, the relationship between their structure and the function they express (i.e., the color) is not yet fully understood:[1] in particular, it is not clear what structural (e.g., geometry and chemical composition) and ambient (e.g., solvation, pH, and temperature) conditions mostly affect the color of a dye.

On the theoretical side, computer simulations based on (time-dependent) density functional theory (DFT, TDDFT) are greatly enhancing our ability to understand, model, and engineer the properties and processes of materials occurring at the atomic scale. A standard approach adopted in the literature consists of the simulation of the optoelectronic properties of the dye in terms of their absorption/emission optical transitions in the gas phase. However, the typical working conditions of such dyes, both in nature and in many biomedical and industrial applications, entail their solvation in a *liquid* environment (e.g., water) at room temperature. It is well-known, for instance, that the polarity and the acidity of the solution may modify the color of the dye (solvatochromic effect):[2] the question then naturally arises as to which extent the structural, electronic, and optical properties of the active molecule are affected by the thermal and dielectric effects induced by the solvent. An explicit quantum mechanical account of the solvent on the optical properties of a solvated molecule has long been considered too demanding computationally. For this reason, the screening effects of the solvent are often treated implicitly using a so-called *polarizable continuum model* (PCM)[3] while disregarding the effects of intermolecular interactions and of intramolecular thermal fluctuations on the absorption spectrum.

In this paper, we consider the effects of intramolecular thermal fluctuations and of intermolecular interactions with the water solvent on the optical properties and color of an anthocyanin dye that we choose as a simple, well-controlled, and paradigmatic example. Anthocyanins are glycosylated derivatives of a 2-phenylbenzopyrylium ($C_6C_3C_6$) core that includes two benzoyl rings separated by a heterocyclic ring (see Figure 1). Different lateral functional groups, such as, e.g., methyl and/or hydroxyl, give anthocyanins with different intrinsic properties.[4] Cyanidin-3-glucoside or *cyanin* (Cya) is a specific anthocyanin characterized by the presence of −OH terminations as lateral groups. In living biological environments, these molecules exist in water solution at very acidic conditions (pH < 3) and are found in a positively charged state, known as *flavylium*. Neutrality is typically restored by the presence of counterions in the solvent.

Traditionally, anthocyanins are studied in the fields of phytochemistry and agriculture because of their reddish-purple dye activity in many plants, flowers, and fruits.[4] In fact, along with chlorophylls (green) and carotenoids (yellow-orange), anthocyanins are one of the most important families of natural dyes. Cyanin, in particular, is responsible for the red to dark-purple
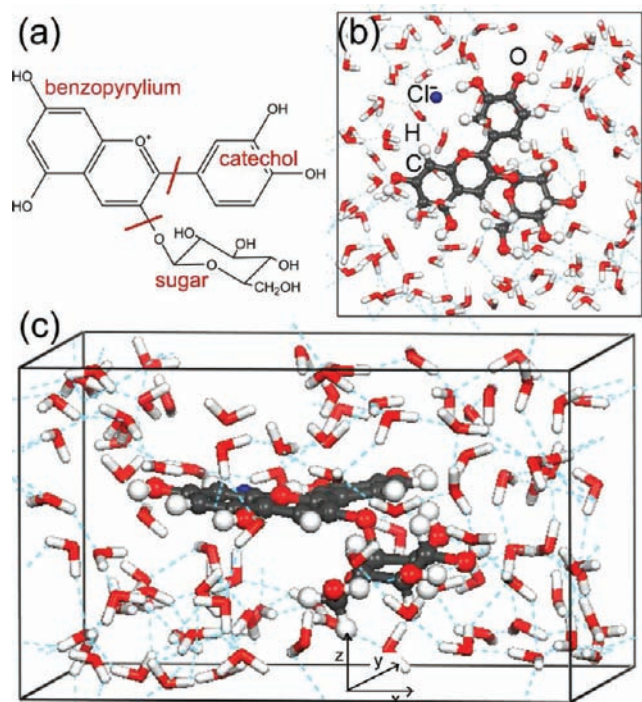
Figure 1. (a) Schematic of the cyanin molecule in the flavylium configuration. Top (b) and side (c) view of the solvated Cya molecule in the simulation cell. Different colors identify different chemical species as specified in panel (b). The H-bonding network is described by dashed lines.

coloration in many vegetables and fruits (such as berries, black grapes, aubergines, etc.[5−9]). Darker purple hues are determined by a strong and broad absorption band extending all over the visible range, possibly depleting at the (blue and red) extrema of the range, while a further depletion at long wavelengths would turn the hue to brighter red. Thus, the exact nuance and brightness that a same dye expresses in different biological systems may depend on such environmental conditions as the pH or the presence of metal ions and copigmentation aggregates,[4,5] which can modify the absorption edge of the molecule. Besides the pigmentation activity, its antioxidant properties and its capability of absorbing UV and visible radiation make cyanin particularly interesting for novel pharmaceutical (e.g., anticancer)[10−15] and nanotechnological applications, respectively. For instance, it has been proposed that Cya may be used as molecular sensitizers in ion-free solar cells.[16−21] The electronic and optical properties of Cya,[20,22] as well as of other flavonoids,[23] have been recently simulated in the gas phase, using (TD)DFT.

In this paper, we study the optical properties of the hydrated cyanin dye, aiming at disentangling the screening effects of the solvent from those of intramolecular thermal fluctuations and of intermolecular interactions. To this end, we start from a previous calculation made for the isolated molecule at zero temperature.[22] The gas-phase spectrum of the dye is characterized by two peaks in the red and in the blue, which would determine a greenish hue incompatible with the dark purple coloration observed in nature. The effects of the solvent are first simulated using a PCM and demonstrated not to change the qualitative features of the spectrum, at least in this approximation, including the greenish hue. We prove that this behavior is not due to the technical details

of the simulation (such as, e.g., the energy functional, the basis set, or the numerical algorithm) but rather to the inadequacy of the PCM to account for the effects of the solvent in terms of static models. Thermal intramolecular and intermolecular interaction effects are then treated explicitly by averaging several spectra calculated on the fly along an ab initio molecular-dynamics (AIMD) trajectory, where the first water solvation shell is treated explicitly at a quantum mechanical level (see Figure 1). The latter step is made possible by recent algorithmic advances in the implementation of TDDFT—based on a Lanczos approach to the linearized quantum Liouville equation, which allows for the calculation of extended portions of the spectrum in systems comprising several hundred atoms.[24,25] Intramolecular thermal fluctuations, as described by our molecular dynamics simulation, are shown to fill the gap between the two main gas-phase absorption peaks, thus substantially enhancing the absorption of visible light and darkening the perceived coloration of the dye. Simulating the dynamics of the molecule in the gas phase results in a brown-reddish coloration, while an explicit account of the interaction with water molecules turns the simulated color toward purple, in agreement with experience.

To rationalize our results, we have calculated the spectra of isolated static molecular models where the catechol and sugar groups were removed and the remaining molecular unit was distorted to mimic intramolecular thermal fluctuations. We find that the absorption spectrum is hardly affected by the removal of the sugar moiety, while it depends quite sensitively not only on the presence of the catechol group but also on its distance and orientation with respect to the benzopyrilium group. This finding allows us to conclude that it is precisely the thermally induced benzopyrilium—catechol bond stretching, bending, and torsion that determine the substantial darkening of dye with respect to the predictions of zero-temperature gas-phase simulations.

■ COMPUTATIONAL DETAILS

Numerical simulations have been performed within DFT and TDDFT, mostly using the PBE[26] generalized gradient approximation (GGA) for the exchange-correlation (XC) functional. For demonstration and benchmarking purposes, a few calculations have also been performed for the isolated flavylium ion using the B3LYP[27] XC functional. The isolated ion has been simulated using codes from the Quantum ESPRESSO,[28,29] octopus,[30] and gaussian09[31] packages (see Supporting Information for numerical details). The latter, in particular, has been used for PCM and B3LYP calculations, whereas octopus has been used for benchmarking purposes. The bulk of the simulations were performed with the cp.x, pw.x, and the turboTDDFT[32] components of Quantum ESPRESSO, all based on the plane-wave pseudopotential method,[33,34] using periodic boundary conditions implemented with a $(20 \times 20 \times 12)$ Å^3 supercell (see Figure 1). In vacuum, the Cya flavylium ion is treated by neutralizing an otherwise charged supercell by a compensating uniform background.[22] The solvated system is simulated by having the molecular ion surrounded by 95 water molecules, mimicking the first solvation shell,[35] while the formal +1 charge of the flavylium cation is neutralized here by including a Cl$^−$ counterion in the simulation cell. The resulting system consists of 339 atoms and 938 electrons. The time evolution of the system is simulated using ab initio molecular dynamics within the Car—Parrinello scheme.[36,37] The system is first thermalized at $T = 300$ K for 3.5 ps using a Nosé-Hoover thermostat,[38,39] starting from a molecular geometry obtained by hydrating the minimum-energy structure of flavylium.[22] The equilibration phase is then followed by 20 ps of production run under constant-energy conditions. Accuracy tests on the choice of the parameters employed for the description of liquid water (e.g., radial
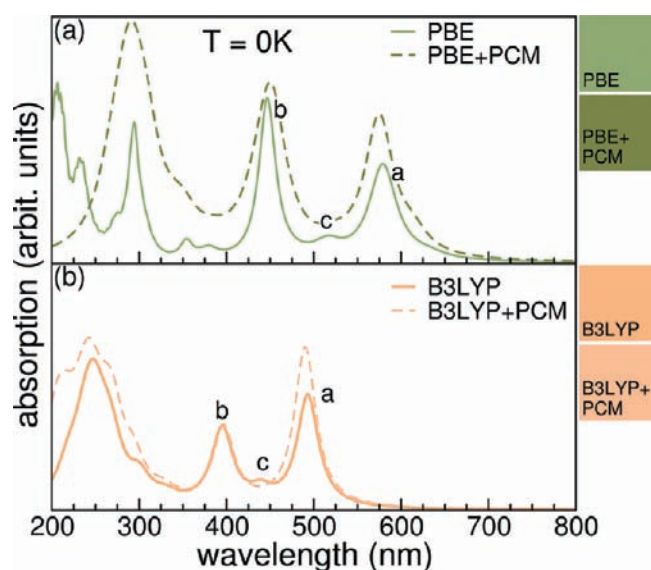
Figure 2. Absorption spectra for the single molecule in the gas phase at zero temperature corresponding to the minimum-energy configuration with (dashed line) and without (straight line) the inclusion of an implicit solvent, obtained with (a) GGA-PBE and (b) hybrid B3LYP exchange correlation functional. The corresponding simulated colors are reported on the right side.

distribution functions, dipole moments, and H-bonds analysis) and of the Cl hydration are reported elsewhere.[35] The absorption spectrum of the solvated ion is simulated by sampling the MD trajectory every picosecond and averaging the resulting spectra calculated on the fly at each snapshot (see also Supporting Information (SI) for accuracy tests). The accuracy of the turboTDDFT code was checked by comparing the UV–vis gas-phase spectra for the molecule in the $T = 0$ K minimum-energy configuration with those obtained from the octopus[30] and gaussian09[31] codes, resulting in an excellent agreement, as reported in Figure S1 of the SI. While being very efficient in the calculation of the absorption spectrum of large systems over a wide frequency range, the Liouville–Lanczos algorithm implemented in turboTDDFT does not allow for a direct analysis of the eigenvectors of the TDDFT Liouvillian corresponding to each spectral feature. Notwithstanding, the linear charge-density response to a perturbing electromagnetic radiation of wavelength λ, $\rho'(\mathbf{r},\lambda)$, can be easily obtained, as explained in ref 32.

Ab Initio Colorimetry. Probably the single most important property of a dye is the color of the light transmitted through a sample of solvated pigment, as perceived by the human eye. A quantitative description of the transmitted color can be obtained from the tristimulus colorimetry theory.[40,41] The RGB representation of the color perceived from a beam of transmitted light, whose spectral distribution is $I_T(\lambda)$, reads

$$RGB = N \int I_T(\lambda) rgb(\lambda) d\lambda \tag{1}$$

where $rgb(\lambda)$ are the three rgb *color-matching* functions (see SI for details), and N is a normalization constant. The spectral distribution of the transmitted light is given by

$$I_T(\lambda) = I_0(\lambda) e^{-\kappa(\lambda)x} \tag{2}$$

where $I_0(\lambda)$ is the distribution of the incident radiation (the *illuminant*), $\kappa(\lambda)$ the absorption coefficient, and x the thickness of the solution sample traversed by the light beam. By using the standard $D65$ illuminant, which mimics the solar spectrum in the visible range (see SI), and RGB color-matching functions provided by the *Commission*

International de l'Eclairage,[42] a semiquantitative estimate of the coloration produced by a given dye can be obtained.[43]

■ RESULTS AND DISCUSSIONS

Gas-Phase and PCM Spectra. Most simulations of the optical properties of complex molecular systems are performed assuming the molecule is in its minimum-energy configuration and possibly accounting for the effects of the solvent using one kind of continuous dielectric model or the other. In the upper panel of Figure 2, we show the absorption spectra calculated for the isolated molecule corresponding to the minimum-energy configuration[22] in vacuum (straight line) or in water solution, as described by a PCM (dashed line), using in both cases a GGA-PBE XC functional. The reported dipolar strength functions are calculated by averaging the dynamical polarizabilities along three independent spatial directions, the individual contributions being highly anisotropic, with the component perpendicular to the π-conjugated plane of benzopyrilyum and catechol almost 1 order of magnitude weaker than the in-plane components.

The PBE spectrum for the gas-phase configuration is dominated in the visible range by two main and sharp peaks at $\lambda = 579$ nm (a) and $\lambda = 452$ nm (b) and a weaker feature at $\lambda = 512$ nm (c), in agreement with previous calculations.[22] The comparison between experimental and theoretical results is more subtle because experimental data for the gas phase are not available. The absorption spectrum for the Cya molecule in water solution at room temperature[17,22] presents a broad band all over the visible range, characterized by two prominent peaks at 512 and 429 nm. Hence, the comparison with the gas-phase spectrum denotes differences both in the shape (broad band versus sharp line) and in the position of the lowest energy peaks that are blue-shifted by ∼20–70 nm with respect to the simulated ones. The latter behavior is partly to be ascribed to the GGA XC functional adopted in the calculations reported above, which notoriously underestimates optical gaps. Furthermore, we notice that the experimental data for the flavylium phase are collected at very acidic conditions, which are known to cause a strong bathochromic shift in the optical spectra because of the presence of the buffer solutions used to control the pH.

We consider the rendering of the molecular color, as perceived by the human eye, starting from our ab initio results. By applying the methodology described in a previous section, the $T = 0$ K absorption spectrum of the molecule in the gas phase would result in a greenish coloration (Figure 2a, right panel), which strikingly contrasts with the red-to-purple pigmentation activity of Cya in biological systems. The question then naturally arises as to whether this failure is due to the inaccuracy of the PBE XC functional or rather to missing the effects of the surrounding solvent. To unravel this problem we consider the dielectric effect of water by means of the inclusion of an implicit PCM solvent (Figure 2a, dashed line), resulting in a slight increase of the absorption intensity, while leaving the position of the main peaks almost unaffected. A shoulder of low oscillator strength appears at 630 nm, which slightly shifts the adsorption edge toward higher wavelengths (bathochromic effect). A similar small solvent effect on the static absorption spectrum has been reported also in the case of other flavonoids (apigenin).[23] The inclusion of a PCM does not correct the wrong perceived color simulated above, only imparting a darker hue to the greenish color previously obtained (Figure 2a).

15427

dx.doi.org/10.1021/ja201733v |*J. Am. Chem. Soc.* 2011, 133, 15425–15433

To ascertain the impact of approximate XC functionals on the optical properties, we finally calculate the absorption spectra, with and without PCM solvent, for the same $T = 0$ K Cya configuration, by using a hybrid B3LYP XC functional. The results are reported in Figure 2b. As expected, the use of a hybrid functional determines an overall blue shift of the spectrum of ~85 nm (~360 meV), while it does not change the shape nor the number of spectral features displayed by the GGA spectrum in the visible range. As expected, the lowest-energy a and b structures are shifted toward smaller wavelengths, closer to the experimental values. On the contrary, the inclusion of PCM hardly affects the overall shape of the spectrum, giving only a small increase of the absorption intensity (hyperchromism), similarly to the PBE case.

The shift of the absorption peaks leads to a modification of the simulated color that turns toward light-orange/pink tones, still far away from dark purple-reddish color expected from experimental evidence. We conclude that the better account of XC effects provided by the B3LYP functional, while improving the description of the spectrum in the gas phase, does not explain the failure of GGA-TDDFT to predict the dark coloration of the dye in a natural wet environment, that can only be due to a denser and less structured spectrum than predicted so far.

Combining TDDFT with AIMD. The failure of the PCM to account for the qualitative features of the optical spectrum of flavylium responsible for its dark coloration suggests that the latter may be due to dynamical effects on the structure of the dye and on its interaction with the solvent, which are missed by the static picture underlying PCM simulations. To properly account for these effects, we combine a description of the structural properties of the dye interacting with the explicit model for the water solvent,[44] based on AIMD, with a description of its optical properties based on TDDFT, as explained in a previous section.

In the time range of our production run, the Cya molecule maintains its main structural configuration: no events involving the formation or breaking of chemical bonds are detected. However, the molecule does undergo severe geometrical distortions, mainly involving torsions, stretchings, and bendings of the catechol and sugar units with respect to the benzopyrilyum one.

The electronic structure of the solvated Cya in the presence of the Cl$^-$ counterion and water molecules has been examined in a previous work.[35] The frontier orbitals of the system have a π-character and are mainly delocalized over the benzopyrylium and catechol rings, whereas the sugar moiety as well as water and Cl$^-$ contribute to the lower-energy part of the single-particle spectrum (~1.0 eV below HOMO). The interplay with water is highly anisotropic and involves both in-plane attractive interactions with the lateral −OH groups of Cya and out-of-plane repulsive interactions due to the coupling with the π orbitals of the conjugated rings. A complete analysis of the first hydration layer and of the ground-state electronic properties is reported in ref 35. Here we focus on the optical properties of the solvated molecule.

Figure 3 displays the time-averaged spectra of the molecule, collected at $T = 300$ K. Three different spectra are reported: "solvated" indicates the time average of the spectra of the solvated molecule; "dehydrated" indicates the average of the spectra for the molecular geometries resulting from the AIMD trajectory of the solvated system but calculated upon removal of the water molecules; "gas 300 K" indicates the time average of the spectra calculated along an AIMD trajectory performed for the isolated molecule. The time-averaged solvated spectrum
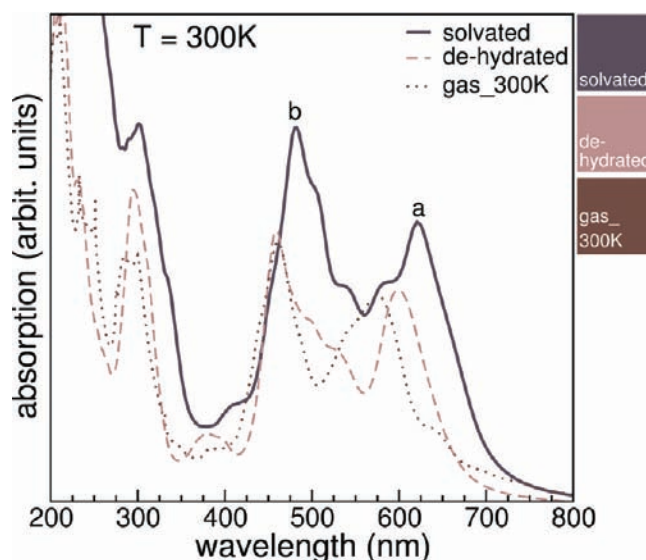

Figure 3. Time-averaged absorption spectra for the Cya molecule at $T = 300$ K for the fully solvated (solid line), the dehydrated (dashed line), and the gas-phase (dotted line) system. The corresponding simulated colors are reported on the right side.

(straight line, Figure 3) features a broader absorption band with respect to the zero-temperature gas-phase spectrum ($\lambda = 400-700$ nm), characterized by two main peaks at $\lambda = 621$ nm (a) and $\lambda = 483$ nm (b) and several shoulders in between. The positions of the maxima (peaks a and b) are quite close in the gas phase at zero temperature, thus giving substance to the practice of comparing spectral features calculated in the gas phase with spectra measured in solution. The overall shape of the spectrum, instead, is completely different, resulting in a much closer resemblance with the experimental one.[17,22] The enhancement of the absorption over a larger spectral range leads to a perceived dark purple color, in agreement with what is observed in nature.

This result shows that it is the use of the PCM to mimic the effects of the solvent, rather than that of an adiabatic GGA DFT functional to describe XC ones, which is responsible for the failure of TDDFT to describe the Cya spectrum in Figure 2. This being the case, the question still remains as to whether the dominant effects missed by PCM simulations are due to the explicit interaction between the optically active dye and the solvent molecules or rather to intramolecular thermal vibrations. To answer this question, we calculated the time average of the spectra for a fictitious dehydrated molecule, obtained from the AIMD trajectory of the solvated system by removing water molecules and the counterion.[45] Note that this is not the time evolution of the gas-phase spectrum because it has not been obtained from the dynamics of the molecule in vacuum. The resulting spectrum (Figure 3, dashed line) is similar to the solvated one, only blue-shifted by ~20 nm, in agreement with PCM results and with the common knowledge about the effect of water solution on the optical properties of organic molecules.[23] This shift is mainly due to the displacement of the low-energy peaks (a) and (b) in the visible range, while the UV portion of the spectrum remains almost unchanged. We also recognize most of the other features (e.g., shoulders) that characterize the solvated spectrum, but are missing in the gas phase. The intensity of the dehydrated spectrum is partially quenched with respect to the fully solvated one. This suggests that water molecules—

interacting with Cya—contribute to the optical response of the system also in the visible region, where pure liquid water is transparent. By comparison with the PCM curve, we conclude that the broadening of the visible absorption band and the presence of its internal structures are due to intramolecular thermal fluctuations and not to any direct hydration effects.

To further confirm this finding, a separate set of AIMD simulations for the Cya molecule in the gas phase (no solvent) evolving in time at room temperature were performed. In the absence of the liquid thermal bath, we first preheated the system at $T = 800$ K for 3.0 ps, and then we thermalized it at $T = 300$K for a further 3.2 ps; finally we collected 20 ps of free dynamics at room temperature. The time-averaged spectrum (labeled "gas_300K") is obtained as before by sampling the trajectory every 1 ps. Results are reported in Figure 3 (dotted line). Similarly to the dehydrated case, the "gas_300K" curve does not include the effect of the solvent, but it differs from the previous curve for the geometries during the dynamics. The two *dry* spectra look similar, having almost the same spectral features especially in the range 300—500 nm. We note, however, a longer tail of the "gas_300K" spectrum beyond ~700 nm, which corresponds to a red-shift of the absorption edge. This effect is due an overbending of the molecule that is no more spatially constrained by the surrounding liquid water (see below). The comparison between the gas-phase spectra taken at zero (Figure 2) and room (Figure 3) temperature demonstrates that the broadening of the spectrum is mainly due to intramolecular thermal fluctuations rather then to the effects of the liquid solvent. Incidentally, the time-averaged spectrum obtained cooling the temperature to 70 K presents a two-peak structure similar to the static configuration at $T = 0$ K. Hereafter, we label as *gas phase* the single Cya molecule in vacuum at zero temperature, in its minimum-energy configuration.

As a further validation of our findings, we simulate the color corresponding to all the time-averaged spectra. As observed before, the spectrum of the solvated molecule corresponds to a dark purple coloration. The spectra of the other two dehydrated and "gas_300K" molecular models give similar but lighter hues. The darker color of the fully solvated system is mainly due to the larger intensity rather than the red-shift of the absorption spectrum. Even though the final color of Cya in biological systems depends on many factors (such as concentration, pH, impurities, etc.), our results indicate that the bare inclusion of solvent effects through implicit models only partially accounts for the dielectric effects of the liquid water (e.g., bathochromic shift) but not for the main features of the absorption spectrum of the solvated molecule, which can instead be properly described only by explicit solvent models.

The adoption of a hybrid XC functional in both AIMD and TDDFT calculations would likely result in a better agreement with experiments. The current implementation of TDDFT in the turboTDDFT code,[32] thanks to which we can afford the calculation optical spectrum of such a large system over an extended lapse of time, is however presently limited to local and semilocal functionals.

Snapshot Analysis. Various structural configurations occurring along the molecular dynamics trajectory lead to absorption spectra which differ remarkably from each other. In this section, we analyze the origin of these differences in terms of dynamical variations of the molecular geometry. All the calculated absorption spectra for the single snapshots are reported in the SI. Here we limit ourselves to two representative configurations, extracted
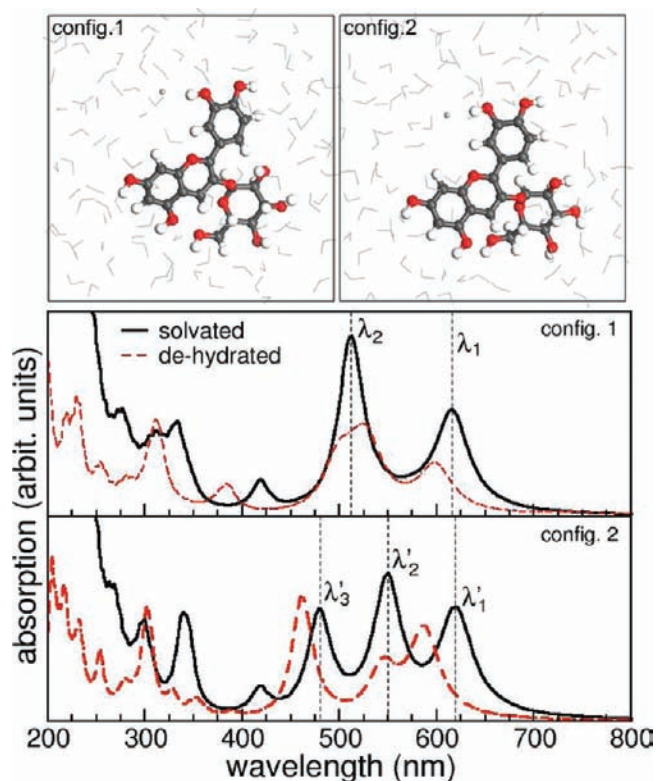

Figure 4. (Top) Atomic structure of cyanin in the two configurations discussed in the text, namely, *config.1* and *config.2*. The counterions and water molecules are drawn in gray scale for clarity. (Bottom) Absorption spectra for two selected snapshots from AIMD trajectory, with (straight lines) and without (dashed lines) solution. Vertical dotted lines identify the low-energy peaks for the solvated configurations, discussed in the text.

from the AIMD trajectory, which are shown in Figure 4 and which we label in the following as *config.1* and *config.2*.

As shown in the top panel of Figure 4, the two configurations look structurally very similar, even though the local geometry features differ for bond lengths and angles. For instance, the distance and the torsion angle between the phenylbenzopyrylium and catechol subunits change only 0.06 Å and ~5°, respectively (see SI for details on the atomic structure). Yet, the comparison between the two spectra highlights remarkable differences: the most evident is the appearance of a third peak in the visible range in *config.2*, which is absent in *config.1*. Also, these low-energy peaks appear at different wavelengths. For the same snapshots, we calculated the spectra for the corresponding dehydrated configurations (Figure 4, dashed line). In both cases, the presence of the solution (water and counterion) induces a hyper- and batho-chromic effect on the spectra, while it does not change the main shape of the curves nor the number of peaks of each configuration, in agreement with the analysis presented above. Since the number of these features does not depend on the presence of the solvent, their origin has to be ascribed to the different atomic structure of cyanin during the dynamics.

To investigate the effect of the different molecular subunits (Figure 1) on the optical spectra of the two sample configurations, we considered systems where selected groups of atoms were taken out: leaving all other atoms fixed (including the solvent molecules), we removed either the sugar
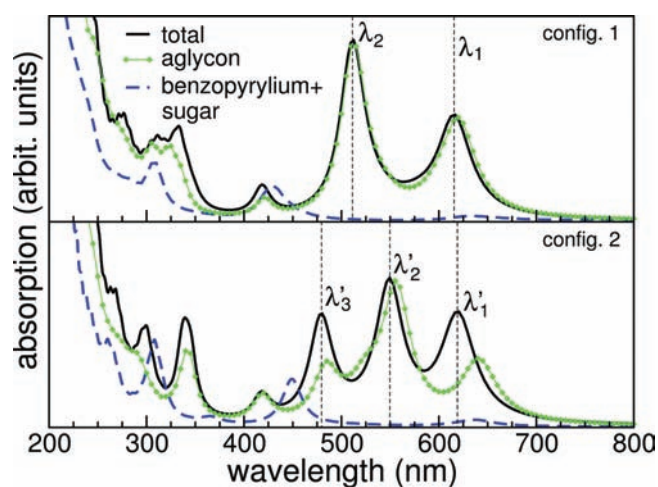
15429

dx.doi.org/10.1021/ja201733v |*J. Am. Chem. Soc.* 2011, 133, 15425–15433

Figure 5. Absorption spectra for aglycon (green dotted lines) and benzopyrylium + sugar (blue dashed lines) subsystems, extracted from the *config.1* and *config.2* geometries. Absorption spectra for the entire systems (black straight lines) are replicated from Figure 3 for clarity.
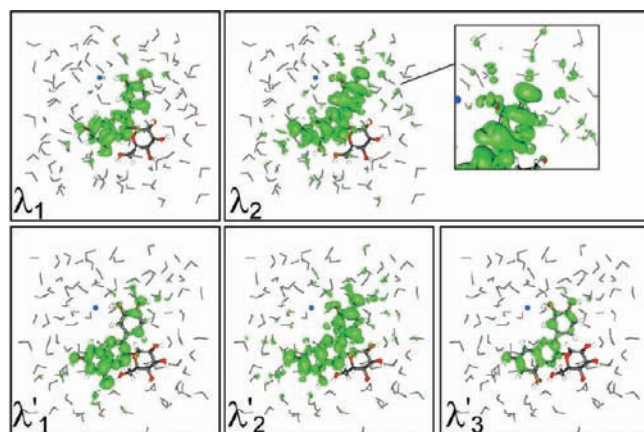

Figure 6. Spatial averaged response charge density, corresponding to the wavelengths defined in Figure 3, for *conFigure 1* (top panel) and *conFigure 2* (bottom panel), respectively. The inset in the upper panel highlights the catechol/water interface.

moiety (aglycon structure or *cyanidin*) or the catechol group (benzopyrylium + sugar). The resulting spectra are reported in Figure 5. For a given configuration, the removal of the sugar group does not affect the main properties of the absorption spectra, thus indicating that sugar has only minor effects on the optical properties of the flavylium cation. On the contrary, the removal of the catechol group changes dramatically the optical response of the molecule, suppressing all absorption in the visible range.

The relative importance of the sugar and catechol subunits is confirmed by an analysis of the electronic response at selected wavelengths. Figure 6 shows the imaginary (absorptive) part[46] of the response charge density $\rho(\mathbf{r},\lambda)$ resulting from the TDDFT calculations, for the two configurations at the wavelengths $\lambda_{1,2}$ and $\lambda'_{1,2,3}$ (see Figure 4). The response charge density plots are representative of the spatial localization of the dipole induced by the incoming electric field (i.e., light) at a given frequency. For all the analyzed peaks, the main contribution to $\rho(\mathbf{r},\lambda)$ stems from

intramolecular excitations. Its spatial distribution is consistent with the coupling of π molecular orbitals, delocalized over the benzopyrylium and catechol rings. Contrastingly, the sugar moiety only partially contributes to the absorption spectra in the visible range, in agreement with the aglycon results of Figure 5a and with the previous discussion.

A closer inspection of Figure 6 shows a small but not negligible contribution to absorption deriving from the water molecules near the flavylium molecule (see inset). This fact is consistent with the differences between the fully solvated and dehydrated spectra (Figure 3). Notably, since the first solvation shell is highly anisotropic,[35] only the lateral H_2O molecules, close to Cya hydroxyl groups, are directly involved in the charge-density response to light excitation. Also note that the first neighboring H_2O molecules in the direction perpendicular to the plane of conjugated rings do *not* contribute to the optical response. The position and number of water molecules changes in time along the AIMD trajectory, thus giving varying contributions to the absorption spectra, as shown by Figure 4. A detailed description of such microscopic effects requires the explicit treatment of the entire system (molecule, solvent and counterions) and is thus not accessible to implicit models of solvation. Finally, we remark that the Cl^- counterion does not take part in the optical activity of the system in the visible range.

From the above analysis, we conclude that: (i) the active chromophore consists of the entire aglycon subsystem, i.e., the 2-phenylbenzopyrylium ($C_6C_3C_6$) core, which acts as a unique π-conjugated system; (ii) the aqueous solution and the sugar group influence the optical spectra only in an indirect way, by changing the polarization of the environment (dielectric effect) and constraining the dynamics of the molecule (geometrical effect); only few water molecules contribute directly to the optical absorption in the visible range; (iii) the main difference between the spectra of the ($T = 0$) isolated and solvated molecules is due to the two main absorption peaks in the gas phase that move and possibly split as a result of thermal fluctuations, thus filling the gap between them on the average; and (iv) this filling effect is achieved by bond bendings and stretchings that, though never determining dramatic changes in the molecular conformation, affect the entire molecule and modify its local electronic structure as well as the coupling with the perturbing electromagnetic field.

Analysis of Geometrical Distortions. In order to better characterize and understand the interplay between geometrical distortions of the molecule and its spectral features, we focus now on the simple cyanidin as a reference model, obtained by removing the sugar moiety from the molecule. In particular, we consider a few selected structural modifications that involve a different coupling between the benzopyrylium and catechol subunits: (i) the stretching of the C−C bond between catechol and benzopyrylium; (ii) the torsion of the catechol ring around the same C−C bond; and (iii) the bending of the catechol with respect to the benzopyrylium plane (Figure 7a).

In the absence of the attached sugar, the molecule is completely planar in its minimum-energy configuration.[22] The corresponding spectrum (thicker lines Figure 7) is very similar to the gas-phase spectrum of Cya with two main peaks at $\lambda = 579$ nm (labeled *a*, as in Figure 2) and $\lambda = 452$ nm (labeled *b*). The two curves differ for the absence in the aglycon spectrum of the contribution at $\lambda = 512$ nm, which is substituted by a shoulder at 550 nm (labeled *c* in Figure 7b).
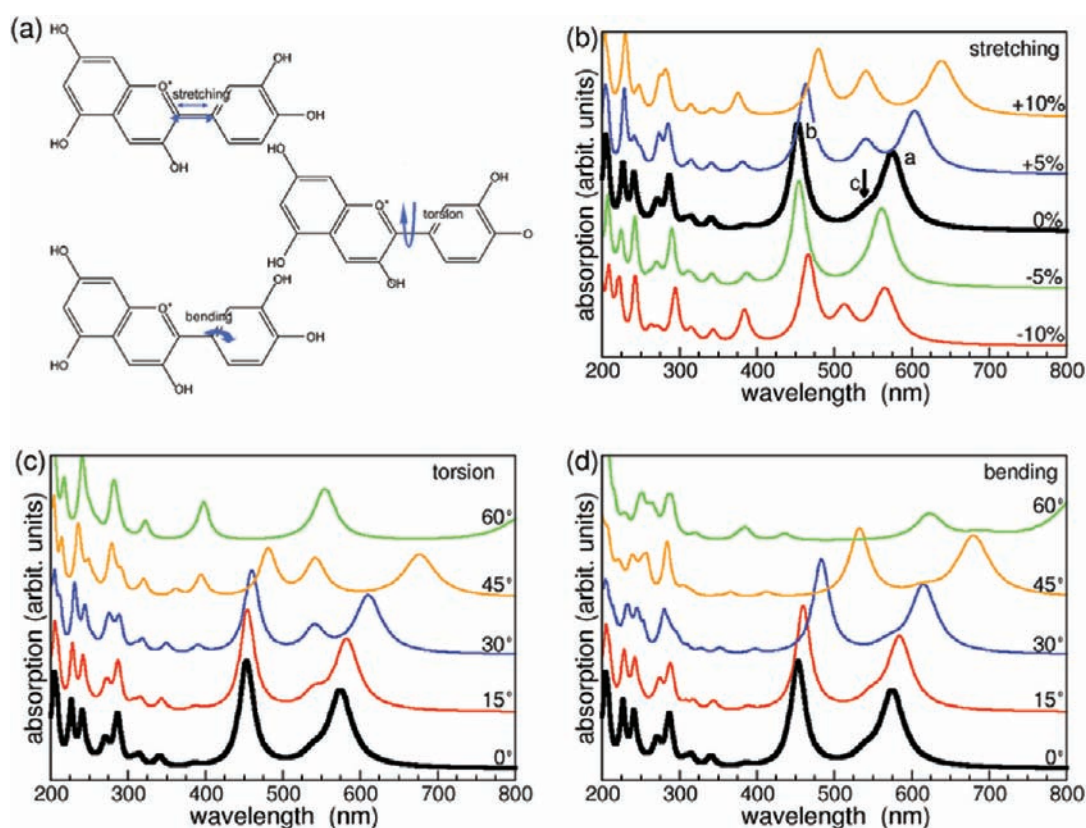
Figure 7. (a) Schematics of the aglycon Cya molecule, indicating the three distortions between benzopyrylium and catechol discussed in the text. Absorption spectra for the aglycon Cya molecule at different (b) stretching, (c) torsion, and (d) bending distortions. Thicker lines in panels b−d correspond to the undistorted cyanidin molecule. Labels *a*, *b*, and *c* in panel (b) identify the two main peaks in the visible range.

The *stretch* of the C−C bond between the benzopyrylium and catechol subunits imparts evident changes in the visible portion of the spectrum. First, passing from −10% to +10% stretching, we observe a red-shift of the entire visible band. Second, as the C−C distance is increased, the wavelength separation between peaks *a* and *b* is strongly increased. Finally, we can detect a third structure appearing between the two main peaks *a* and *b*, whose position is almost fixed. This structure is recognizable either as an isolated peak or as a shoulder, depending on the superposition with the neighboring peaks *a* and *b*.

The effect of the torsional *rotation* of the catechol ring is similar (Figure 7c). We note, however, that in this case the red shift is mostly limited to the lowest-energy absorption peak (*a*). Rotations larger than 45° (which however occurred rarely in our AIMD trajectory) dramatically displace the adsorption edge toward the near-infrared range. The oscillator strength of the central contribution increases with the torsional angle; the opposite occurs for the other two peaks. In the case of the *bending* distortion of the catechol ring out of the benzopyrylium plane (Figure 7d), no splitting of the peaks is observed, while the entire band (two peaks and the shoulder) is shifted toward lower energies.

We conclude that the spectrum of the cyanidin molecule (i.e., the active chromophore of the entire system) is always characterized by three structures in the visible range: two main peaks and a contribution of lower intensity in between. The structural distortions modify the energy and the π-delocalization (i.e., the amount of conjugations across the molecule) of the frontier states that interact in a different way with the incoming light. This causes changes in the mutual energy positions and oscillator strengths of

the three peaks in the visible range. Higher-energy single-particle orbitals (e.g., σ states) are less sensitive to those structural modifications, leaving therefore the UV part of the spectrum almost unchanged.

As the different distortions of the benzopyrylium/catechol units shift and split the spectral features in different ways, the final shape of the spectrum is strongly affected by the structural fluctuations along the trajectory. Even though the origin of these peaks is well understood, the complexity of the molecule (i.e., the high number of degrees of freedom) does not allow one to identify a unique and representative structural parameter whose modification may simply explain the differences in the optical spectra during the dynamics. Thus, the spectral features lying between the peaks *a* and *b* sometimes emerge as one isolated peak (like in *config.2*), sometimes appear as a shoulder of the *a*−*b* peaks, or are completely hidden due to the overlap with one of the higher-intensity peaks nearby, as in *config.1*. We finally checked that this behavior is independent of the choice of the XC functional. Indeed, the use of a hybrid XC functional would result in a quasi-rigid shift of the calculated spectra toward lower wavelengths, while the dependence of individual spectral features on the local molecular geometry would be the same as observed using the PBE functional used in our AIMD simulation and in the previous analysis (see Figure S5, SI).

■ CONCLUSIONS

The main result of our study is the demonstration that the optical activity of natural dyes may dramatically depend on the

dynamical modifications of the molecular configuration induced by thermal fluctuations. No static model can properly describe these effects, not even if the dielectric screening of the solvent is implicitly accounted for by a polarizable continuum model. When this is the case, an explicit account of thermal fluctuations via molecular dynamics and of the effects of the solvent via the explicit inclusion of water molecules in the molecular model of the system is in order. The computation of the optical spectrum by time averaging the spectra calculated on the fly over a molecular trajectory is a daunting task, which can however be addressed using recent developments in the implementation of (linearized) time-dependent density-functional theory. A major issue to be addressed and understood is the extent to which the optical properties calculated for static, minimum-energy configurations of the isolated molecule are robust with respect to the combined effects of thermal fluctuations and the interaction with the solvent molecule. This will certainly be the theme for further systematic investigations.

■ ASSOCIATED CONTENT

ⓢ Supporting Information. Accuracy tests, details on tristimulus colorimetry, single snapshot spectra, and atomic structure of *config.1* and *config.2*, discussed in the text. Complete refs 29 and 31. This material is available free of charge via the Internet at http://pubs.acs.org.

■ AUTHOR INFORMATION

Corresponding Author
arrigo.calzolari@nano.cnr.it

Present Addresses
#Centro S3, CNR-Istituto di Nanoscienze, I-41125 Modena, Italy

■ ACKNOWLEDGMENT

■ REFERENCES

(1) Griffiths, J. *Colour and Constitution of Organic Molecules*; Academic Press Inc.: New York, 1976; pp 240–270.

(2) Reichardt, C. *Chem. Rev.* **1994**, *94*, 2319–2358.

(3) Tomasi, J.; Mennucci, B.; Cammi, R. *Chem. Rev.* **2005**, *105*, 2999–3094.

(4) Brouillard, R. Flavonoids and flower color. In *The Flavonoids*; Harborne, J. B., Ed.; Chapman and Hall Ltd.: London, 1988; pp 525–538.

(5) Harborne, J. B. In *Comperative Biochemistry of the Flavonoids*; Academic Press: New York, 1967; pp 1–99.

(6) Timberlake, C. F.; Bridle, P.; Mabry, P. T. J.; Mabry, H. In *The Flavonoids*; Academic Press: New York, 1975; pp 214–256.

(7) Mazza, G.; Brouillard, R. *Food Chem.* **1987**, *25*, 207–225.

(8) Gonnet, J.-F. *Food Chem.* **2001**, *75*, 743–485.

(9) Parry, J.; Su, L.; Moore, J.; Cheng, Z.; Luther, M.; Rao, J. N.; Wang, J.-Y.; Yu, L. L. *J. Agric. Food Chem.* **2006**, *54*, 3773–3778.

(10) McGhie, T. K.; Walton, M. C. *Mol. Nutr. Food Res.* **2007**, *51*, 702–713.

(11) Mulinacci, N.; Romani, A.; Pinelli, P.; Gallori, S.; Giaccherini, C.; Vincieri, F. F. *Int. J. Pharm.* **2001**, *216*, 23–31.

(12) Harborne, J.; Williams, C. A. *Phytochemistry* **2000**, *55*, 481–504.

(13) Kong, J.-M.; Chia, L.-S.; Goh, N.-K.; Chia, T.-F.; Brouillard, R. *Phytochemistry* **2003**, *646*, 923–933.

(14) de Pascual-Teresa, S.; Sanchez-Ballesta, M. T. *Phytochem. Rev.* **2008**, *7*, 281–299.

(15) Galvano, F.; La Fauci, L.; Lazzarino, G.; Fogliano, V.; Ritieni, A.; Ciappellano, S.; Battistini, N. C.; Tavazzi, B.; Galvano, G. *J. Nutr. Biochem.* **2004**, *15*, 2–11.

(16) Cherepy, N. J.; Smestad, G. P.; Zhang, M. G. J. Z. *J. Phys. Chem. B* **1997**, *101*, 9342–9351.

(17) Hao, S.; Wu, J.; Huang, Y.; Lin, J. *Sol. Energy* **2006**, *80*, 209–214.

(18) Sirimanne, P.; Senevirathna, M.; Premalal, E.; Pitigala, P.; Sivakumar, V.; Tennakone, K. *J. Photochem. Photobiol. A: Chem.* **2006**, *177*, 324–327.

(19) Wongcharee, K.; Meeyoo, V.; Chavadej, S. *Sol. Energy Mater. Sol. Cells* **2007**, *91*, 566–571.

(20) Meng, S.; Ren, J.; Kaxiras, E. *Nano Lett.* **2008**, *8*, 3266–3272.

(21) Rocca, D.; Gebauer, R.; De Angelis, F.; Nazeeruddin, M. K.; Baroni, S. *Chem. Phys. Lett.* **2009**, *475*, 49–53.

(22) Calzolari, A.; Varsano, D.; Ruini, A.; Catellani, A.; Tel-Vered, R.; Yildiz, H. B.; Ovits, O.; Willner, I. *J. Phys. Chem. A* **2009**, *113*, 8801–8810.

(23) Amat, A.; Clementi, C.; De Angelis, F.; Sgamellotti, A.; Fantacci, S. *J. Phys. Chem. A* **2009**, *113*, 15118–15126.

(24) Walker, B.; Saitta, A.; Gebauer, R.; Baroni, S. *Phys. Rev. Lett.* **2006**, *96* (113001), 1–4.

(25) Rocca, D.; Gebauer, R.; Saad, Y.; Baroni, S. *J. Chem. Phys.* **2008**, *128* (154105), 1–14.

(26) Perdew, J. P.; Burke, K.; Ernzerhof, M. *Phys. Rev. Lett.* **1996**, *77*, 3865–3868.

(27) (a) Becke, A. D. *J. Chem. Phys.* **1993**, *98*, 5648. (b) Lee, C.; Yang, W.; Parr, R. G. *Phys. Rev. B* **1988**, *37*, 785.

(28) Scandolo, S.; Giannozzi, P.; Cavazzoni, C.; de Gironcoli, S.; Pasquarello, A.; Baroni, S. *Z. Kristallogr.* **2005**, *220*, 574.

(29) Giannozzi, P.; et al. *J. Phys.: Condens. Matter* **2009**, *21* (395502), 1–20.

(30) Castro, A.; Appel, H.; Oliveira, M.; Rozzi, C. A.; Andrade, X.; Lorenzen, F.; Marques, M. A. L.; Gross, E. K. U.; Rubio, A. *Phys. Status Solidi B* **2006**, *243*, 2465–2488.

(31) Frish, M. J. et al. *Gaussian 09*, revision A1; Gaussian Inc.: Wallingford, CT, 2009.

(32) Malcıoğlu, O. B.; Gebauer, R.; Rocca, D.; Baroni, S. *Comput. Phys. Commun.* **2011**, *182*, 1744–1754. turboTDDFT is the TDDFFT component of Quantum ESPRESSO, based on the Liouville—Lanczos approach introduced in refs 24 and 25.

(33) Vanderbilt, D. *Phys. Rev. B* **1990**, *41*, R7892–R7895.

(34) Walker, B.; Gebauer, R. *J. Chem. Phys.* **2007**, *127* (164106), 1–9.

(35) Calzolari, A.; Monti, S.; Ruini, A.; Catellani, A. *J. Chem. Phys.* **2010**, *132* (114304), 1–9.

(36) Car, R.; Parrinello, M. *Phys. Rev. Lett.* **1985**, *55*, 2471–2474.

(37) Pastore, G.; Smargiassi, E.; Buda, F. *Phys. Rev. A* **1991**, *44*, 6334–6347.

(38) Nosé, S. *J. Chem. Phys.* **1984**, *81*, 511–519. and *Mol. Phys.* **1984**, *52*, 255–268.

(39) Hoover, W. G. *Phys. Rev. A* **1985**, *31*, 1695–1697.

(40) Schanda, J. *Colorimetry: Understanding the CIE System*; John Wiley and Sons: Hoboken, 2007.

(41) http://en.wikipedia.org/wiki/CIE_1931_color_space.

(42) CIE - Commission International de l'Eclairage, see also www. cie.co.at.

(43) In practice, we obtained first the so-called XYZ representation of the color of the transmitted light and transformed then the resulting color to the RGB representation, as described, e.g., in refs 40 and 41. See also: Fairman, H. S.; Brill, M. H.; Hammendinger, H. *Col. Res. Appl.* **1998**, *22*, 11–23.

(44) In AIMD, the charge state of the dye and of the counterion is not imposed a priori but results from the dynamical evolution of the quantum mechanical state of the system.

15432

dx.doi.org/10.1021/ja201733v |*J. Am. Chem. Soc.* 2011, 133, 15425–15433

(45) We checked that the use of compensating jellium, adopted to neutralize the positive charge of avylium, does not affect the TDDFT results.

(46) In the frequency (or wavelength) domain, the response charge density is a complex function, whose imaginary part is related to the absorption coefficient; see, e.g., ref 32.

15433

dx.doi.org/10.1021/ja201733v |*J. Am. Chem. Soc.* 2011, 133, 15425–15433